Nanoindentation and the dynamic characterization of viscoelastic solids



2008 J. Phys. D: Appl. Phys. 41 074021

(http://iopscience.iop.org/0022-3727/41/7/074021)

IOP PUBLISHING JOURNAL OF PHYSICS D: APPLIED PHYSICS

J. Phys. D: Appl. Phys. **41** (2008) 074021 (9pp) doi:10.1088/0022-3727/41/7/074021

# Nanoindentation and the dynamic characterization of viscoelastic solids

**E G Herbert**[1,2], **W C Oliver**[1,2] **and G M Pharr**[1,3]

[1] The University of Tennessee, College of Engineering, Department of Materials Science and Engineering, 434 Dougherty Engineering Building, Knoxville, TN 37996-2200, USA
[2] MTS Nano Instruments Innovation Center, 701 Scarboro Road, Suite 100, Oak Ridge, TN 37380, USA
[3] Materials Science & Technology Division, Oak Ridge National Laboratory, P.O.Box 2008, Building 4500S, 1 Bethel Valley Road, Oak Ridge, TN 37831-6132, USA

Received 17 August 2007, in final form 17 October 2007
Published 12 March 2008
Online at stacks.iop.org/JPhysD/41/074021

**Abstract**
Using a high-damping thermoplastic as a standard reference material, the purpose of this work is to compare measured values of the complex modulus as determined by dynamic nanoindentation and dynamic mechanical analysis (DMA). Experiments were performed at approximately 22 °C and seven frequencies over the range 1–50 Hz. The indentation measurements were performed using a 103 $\mu$m diameter flat punch and a newly developed test method that optimizes the accuracy and precision of the measured stiffness and damping. As determined by dynamic nanoindentation, values of the storage modulus and loss factor (tangent delta) ranged from 4.2 to 10.2 MPa, and 0.28 to 1.05, respectively. Over the range 1–25 Hz, DMA confirmed the nanoindentation results to within 15% or better. Collectively, these data and the testing methods used to generate them should help future investigators make more accurate and precise measurements of the dynamic properties of viscoelastic solids using nanoindentation.

## 1. Introduction

The attractiveness of nanoindentation is its ability to characterize the mechanical behaviour of small volumes of material with spatial resolutions in the nanometre to micrometre range. Over the past 20 years, the technique has been routinely used to investigate the linear elastic and plastic properties of thin films, modified surfaces, individual phases in alloys and composites and other microscopic features and structures [1, 2]. Attempts to characterize viscoelastic solids, on the other hand, have been far fewer in number, and additionally, most have focused on the strain-rate sensitivity and the transient properties of creep and stress relaxation [3–12]. Among the reasons for the large gap between dynamic elastic and dynamic viscoelastic indentation data in the open literature is the added complexity of performing meaningful experiments in the frequency domain. Loubet and Lucas were the first investigators to use dynamic nanoindentation to investigate the frequency response of polymers [13, 14]. As they emphasized, accurate experimental techniques are entirely dependent on rigorous dynamic characterization of the measurement system itself. In addition, experimental data are most frequently modelled such as to be representative of steady-state harmonic motion, a known contact geometry, and in many cases, linear viscoelasticity. Only under these conditions are the storage and loss modulus uniquely related to the transient functions from which the material parameters are derived, namely, creep and stress relaxation.

Among the investigations that have used dynamic nanoindentation to measure the complex modulus, notable contributions have been made by Odegard and White [15–17]. In both cases, the investigators present a direct comparison of results generated by nanoindentation and dynamic mechanical analysis (DMA). This comparison is important because it provides a means of assessing the accuracy of the nanoindentation results, since DMA is regarded as the standard testing technique used by many modellers and designers. Odegard and White's results show good agreement between nanoindentation and DMA data for glassy, high modulus materials ($E' \sim 1$ GPa). In contrast, White's results on a rubbery, low modulus material ($E' \sim 1$ MPa) did not match as well; the nanoindentation results overestimated the DMA by nearly a factor of 2.

If nanoindentation is to become a viable characterization tool for the dynamic behaviour of viscoelastic solids, a

 

comparison between nanoindentation and DMA results like that of Odegard and White is needed to demonstrate the strengths and weaknesses of the technique. Additionally, meaningful comparisons must be supported by experimental verification of a steady-state harmonic response, a known contact geometry and linear viscoelasticity. Seemingly simple choices like indenter geometry have a significant impact on the ability to make meaningful measurements, as pyramids, spheres and punches each have their own unique advantages and disadvantages. For example, recent work by Tweedie and Van Vliet [18] found that experiments performed with a pyramidal indenter on a number of polymer materials failed to generate a contact consistent with the assumptions of linear viscoelasticity. Conversely, spheres used in the limit of small displacements relative to the radius of the tip were successful in generating data that accurately describes the linear viscoelasticity in these materials. The message from these investigations is that accurate experimental determination of the complex modulus by nanoindentation requires thoughtful experiments based on the general properties of the material and the choice of indenter geometry. Moreover, the cornerstone of the technique is a rigorous dynamic characterization of the measurement system itself.

The goal of this work is to provide experimental evidence that will help demonstrate the viability of dynamic nanoindentation as a characterization technique for viscoelastic solids. In doing so, a strategy will be established that may be used to ensure the accuracy and precision of dynamic nanoindentation measurements. These objectives are achieved by (1) developing a thorough understanding of the key factors that control the design of robust experiments, (2) demonstrating how these factors can be incorporated experimentally and (3) presenting a direct comparison of complex modulus measurements made on a high-damping thermoplastic using dynamic nanoindentation and DMA.

## 2. Theory

### *2.1. The dynamic response of a linear viscoelastic solid*

For a linear viscoelastic material under sinusoidal loading, the stress–strain relationship may be expressed as

$$\sigma = \varepsilon_o E' \sin \omega t + \varepsilon_o E'' \cos \omega t, \tag{1}$$

where $\sigma$ is the stress, $\varepsilon_o$ is the strain amplitude, $\omega$ is the angular frequency, $t$ is the time,

$$E' = \frac{\sigma_o}{\varepsilon_o} \cos \phi \tag{2}$$

and

$$E'' = \frac{\sigma_o}{\varepsilon_o} \sin \phi, \tag{3}$$

where $\sigma_o$ is the stress amplitude and $\phi$ is the phase lag between the stress and the strain [19]. $E'$ and $E''$ are, respectively, the storage and loss modulus. $E'$ represents the material's capacity to store energy; it is the component in phase with the applied displacement or load. $E''$ represents the material's capacity to dissipate energy; it is the component 90° out of phase with the applied displacement or load. The ratio $E''/E' = \tan \phi$ is called the loss factor and is often used as a measure of damping in a linear viscoelastic material. Collectively, these frequency-dependent properties are used to characterize the viscoelastic response of a material.

It is often useful to analyse the mechanics of viscoelasticity by writing the stress–time and strain–time relationships in their complex forms:

$$\sigma = \sigma_o e^{i\omega t} \tag{4}$$

and

$$\varepsilon = \varepsilon_o e^{i(\omega t + \phi)}. \tag{5}$$

Taking the ratio of stress to strain,

$$\frac{\sigma}{\varepsilon} = \frac{\sigma_o}{\varepsilon_o} e^{i\phi} = E^*, \tag{6}$$

where $E^*$ is called the complex modulus, and in accordance with Euler's identity,

$$E^* = \frac{\sigma_o}{\varepsilon_o}(\cos \phi + i \sin \phi) = E' + iE''. \tag{7}$$

One benefit of casting the relationship in this form is that it allows the complex harmonic motion to be graphically represented by a phasor diagram, which provides a simple interpretation of the relationship between $E^*$, $E'$, $E''$ and $\phi$. The phasor diagram is shown in figure 1(*a*), where $\phi$ is an angle in the complex plane. $E^*$ is the phasor, whose magnitude equals $\sigma_o/\varepsilon_o$, which is also equivalent to $\sqrt{E'^2 + E''^2}$. In accordance with equation (7), the $x$- and $y$-axes represent, respectively, the real (elastic stress) and imaginary (viscous stress) components of the complex modulus. The value of the phasor diagram here is that it helps provide physical insight in developing robust indentation experiments to measure the complex modulus of viscoelastic solids.

### *2.2. The dynamic response of a damped, forced oscillator—the test instrument*

Figure 2(*a*) shows a schematic illustration of the instrument used to perform the dynamic nanoindentation testing and its corresponding dynamic model. In response to a sinusoidally varying force, the differential equation which describes the motion of the system is

$$F_o e^{i\omega t} = m\ddot{h} + C\dot{h} + Kh, \tag{8}$$

where $F_o$ is the amplitude of the load oscillation, $m$ is the mass of the indenter, $h$ is the displacement response, $C$ is the damping coefficient of the instrument and $K$ is the stiffness of the support springs. Since equation (8) is nonhomogeneous, the general solution is the sum of a complimentary solution and a particular solution. The particular solution, which describes the steady-state motion of the system, is assumed to be

$$h(t) = h_o e^{i(\omega t - \phi)}, \tag{9}$$

where $h_o$ is the amplitude of the displacement oscillation. Thus, the displacement oscillates at the same frequency as the

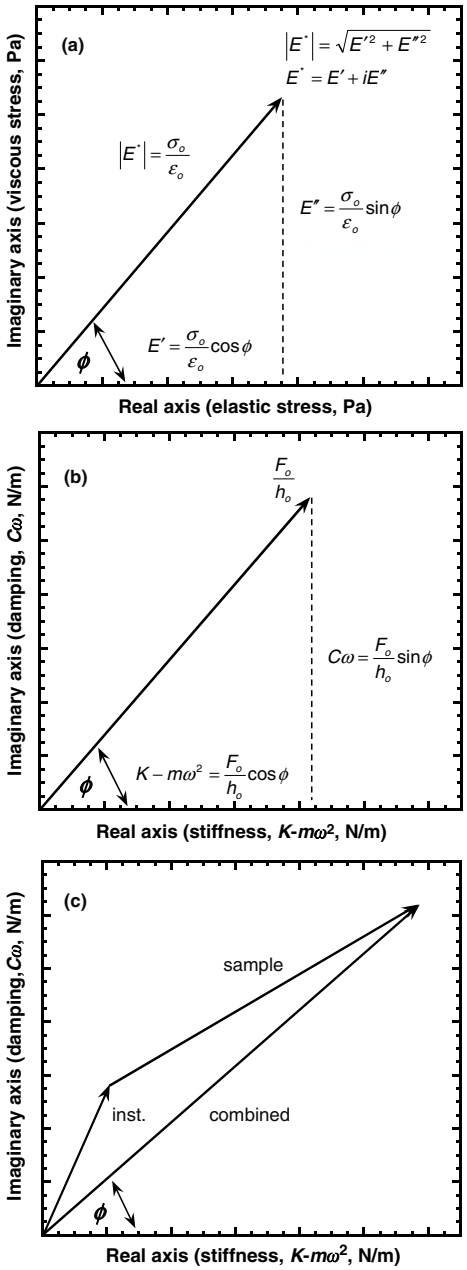


**Figure 1.** Schematic illustrations showing the imaginary and real components of (*a*) the complex modulus of a linear viscoelastic solid subject to sinusoidal loading, (*b*) the frequency response of a damped, forced oscillator and (*c*) the combined frequency response of a viscoelastic solid (sample) and a damped, forced oscillator (instrument).

applied force but potentially lags behind by the phase angle. By substituting the necessary time derivatives and simplifying equation (8), the real and the imaginary components can be equated to solve for the magnitude of the dynamic compliance of the system,

$$\frac{h_o}{F_o} = [((K - m\omega^2)^2 + \omega^2 C^2)^{1/2}]^{-1}. \tag{10}$$

Additionally, the phase angle between the applied load and the resulting displacement is given by

$$\tan\phi = \frac{C\omega}{K - m\omega^2}. \tag{11}$$

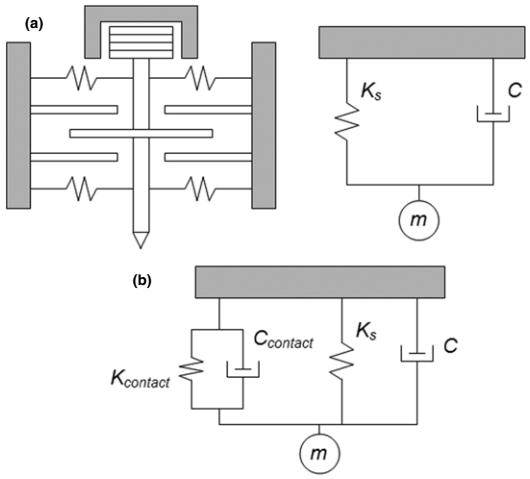


**Figure 2.** (*a*) A schematic illustration of the testing system and the dynamic model used to describe the behaviour of the system as a function of frequency. (*b*) The dynamic model used to describe the combined frequency response of the instrument and sample. Throughout this work, the load frame is assumed to be rigid relative to the stiffness of the support springs, $K_s$.

Using equations (10) and (11), the dynamic stiffness, $K - m\omega^2$, and damping, $C\omega$, of the instrument are found to be

$$K - m\omega^2 = \frac{F_o}{h_o}\cos\phi \tag{12}$$

and

$$C\omega = \frac{F_o}{h_o}\sin\phi. \tag{13}$$

Analogous to figure 1(*a*), the dynamic response of a damped, forced oscillator may also be represented by a phasor diagram. Figure 1(*b*) illustrates the instrument's frequency response in the complex plane and shows the relationships between $K - m\omega^2$, $C\omega$, $\phi$ and $F_o/h_o$. As shown in the figure, $F_o/h_o$ is the magnitude of the phasor representing the frequency response of the instrument and $\phi$ is an angle in the complex plane. The $x$- and $y$-axes represent the real (stiffness) and imaginary (damping) components of the displacement response of the system. Although the axes in figures 1(*a*) and (*b*) are fundamentally different, they are uniquely related through the geometry of the contact.

### *2.3. Determining E′ and E″ in a dynamic nanoindentation experiment*

For a load controlled testing system, the force amplitude is set and the resulting displacement amplitude and phase angle are measured. When the indenter and sample, which are coupled through the geometry of the contact, undergo steady-state harmonic motion, the measured stiffness (equation (12)) and damping (equation (13)) represent the combined frequency response of the instrument and the sample. The dynamic stiffness and damping of the contact (i.e. material response and parameters) are determined by subtracting out the instrument's contribution to the total measured response. It is important to note, however, only in the limit that the additional moving mass of the sample is small in comparison with the mass of

the column do the $m\omega^2$ terms cancel. In other words, the inertial contribution of the sample is assumed to be negligible in comparison with the testing system. In the limit of linear viscoelasticity, the elastic–viscoelastic correspondence principle is deemed valid and thus Sneddon's stiffness equation, the fundamental equation of nanoindentation, may be used to relate the dynamic stiffness and damping of the contact to $E'$ and $E''$ [20],

$$\frac{E'}{1-\nu^2} = \frac{F_o}{h_o}\cos\phi\frac{\sqrt{\pi}}{2}\frac{1}{\beta}\frac{1}{\sqrt{A}} \tag{14}$$

and

$$\frac{E''}{1-\nu^2} = \frac{F_o}{h_o}\sin\phi\frac{\sqrt{\pi}}{2}\frac{1}{\beta}\frac{1}{\sqrt{A}}, \tag{15}$$

where $\nu$ is Poisson's ratio, $\beta$ is a term related to the geometry of the contact and $A$ is the projected contact area. $\beta = 1$ for a circular contact (circular flat punch, sphere and cone), $\beta = 1.034$ for a Berkovich [21]. While Poisson's ratio is physically capable of exhibiting time dependent behaviour, it was assumed to be a constant value of 0.3 for all of the nanoindentation and DMA data analysis presented in this work.

The phasor diagram in figure 1(*c*) can now be used to explain the coupled dynamic response of the sample and the testing system. As previously explained, the frequency response of the instrument is controlled by the magnitude of the moving mass, the stiffness of the support springs and the damping in the head. For a given instrument, these parameters are essentially fixed. The frequency response of the sample is controlled by $E'(\omega)$, $E''(\omega)$ and the geometry of the contact. $E'(\omega)$ and $E''(\omega)$ are fixed for a given material and frequency, and the geometry of the contact can be controlled by using a flat punch indenter. As such, control of the contact geometry is the means by which robust experiments can be designed so that the sample dominates the measured response. In working with constraints such as the available volume of material and microstructure, however, this criterion is not always simple to achieve. Thus, when the instrument's contribution comprises a significant fraction the combined response, it is imperative to know the dynamic stiffness and damping of the instrument as accurately and precisely as possible, since the accuracy of the experimental measurements then relies on isolating small changes in potentially large numbers. As dictated by many applications, this is frequently the condition under which many experiments are performed, i.e. thin films and small volumes of material.

*2.3.1. Modelling the sample.* The dynamic behaviour of viscoelastic solids is most frequently modelled using combinations of linear springs and linear dashpots. The various groupings of springs and dashpots are used to establish the differential equations which describe the material's response to an applied load or displacement. At one end of the spectrum, the Voigt model, a spring and dashpot in parallel, offers the simplest means of describing viscoelastic behaviour, as its response to a sinusoidal input is a sinusoidal output with a phase lag. At the other end of the spectrum, models incorporating more complex assemblages of springs and dashpots may be used to capture more complex material behaviour as a function of frequency. All these models are phenomenological in nature and based on the assumption of linear viscoelasticity. This condition is valid only in the limit of small strains, loosely defined as strains less than 1%.

In this work, the sample was chosen to be modelled as a Voigt solid, as indicated by the 'contact' in figure 2(*b*) (the contact and the instrument are arranged in parallel because they necessarily experience the same change in displacement). This model captures the essence of viscoelastic behaviour and is simple to implement. However, because this model only has the means of incorporating a single relaxation time, it is limited to modelling material behaviour at a single frequency. Furthermore, it has no means of accounting for instantaneous elasticity. While more complex models offer a means to overcome these limitations, experimental evidence is needed to determine the extent of the improvements and the ability to predict the frequency dependence. The recent work of Wright *et al* [22] explores this issue, and develops the rigorous mathematics required to incorporate an additional spring into the Voigt model to allow for instantaneous elasticity.

## 3. Experimental measurements

The storage and loss moduli, $E'$ and $E''$, were measured on a bulk sample of a highly plasticized polyvinyl chloride (PVC), which is a high-damping thermoplastic. The experiments were conducted at frequencies of 1, 3, 5, 10, 20, 30 and 50 Hz. Both the indentation and DMA samples were taken from the exact same sheet of material. The indentation sample measured 8.2 mm long, 6.8 mm wide and 7 mm thick. The precision-machined DMA sample was approximately 35 mm long, 15 mm wide and 5 mm thick. Every effort was made to ensure uniformity in the thickness of the sample, since $E'$ is proportional to the thickness cubed ($E' \propto t^3$). All of the experiments were conducted at approximately 22 °C, which is well above the sample's glass transition temperature of −17.2 °C. For the indentation experiments, the air temperature in the lab was controlled to within ±1 °C using a constant reheat system. The air temperature near the surface of the sample was measured using a precision thermometer. For the DMA experiments, the air temperature was controlled using a liquid nitrogen gas cooling system provided by the instrument manufacturer, TA Instruments.

The nanoindentation experiments were performed on a MTS NanoIndenter® XP using a 103 $\mu$m diameter diamond flat punch in conjunction with a 50 nm oscillation amplitude and the continuous stiffness measurement (CSM) technique. Details of the CSM technique have been described previously [1]. The DMA experiments were performed using a TA Instruments model Q800 and the dual cantilever sample mount, which clamps the sample at both ends. The instrument was completely calibrated in accordance with the procedures provided by TA Instruments. Using polycarbonate as a standard reference material, the measured $E'$ at 1 Hz and room temperature was 2349 MPa, which compares well with the literature value of 2350 MPa. Measurements performed on the PVC at 1 Hz with amplitudes of 20, 40 and 60 $\mu$m generated

data consistent with the assumptions of linear viscoelasticity, as the change in amplitude had virtually no impact on the measured $E'$. As a result, the oscillation amplitude was chosen to be 20 $\mu$m for all DMA experiments performed on the PVC. In addition, the experiments incorporated a thermal soak period of 1 h. All of the averaged nanoindentation and DMA data are presented with error bars spanning one standard deviation about the mean.

The diameter of the flat punch was chosen by design. As previously discussed, important considerations in choosing the tip geometry are (1) the desire to achieve dynamic stiffness and damping measurements that are dominated by the response of the sample and (2) the microstructure of the sample and the available volume of material. The reference material selected for this work is a commercially available, high-damping thermoplastic in bulk form. The material is amorphous and devoid of crosslinking; therefore even small volumes of the material are representative of the bulk microstructure. Using equation (12) and assuming $E'$ at 1 Hz is on the order of 1–10 MPa, $\beta = 1$, and the flat punch has a radius of 50 $\mu$m, the resulting contact stiffness is 100–1000 N m$^{-1}$, which is approximately 1–10 times larger than the stiffness of the instrument's support springs. The fact that the instrument stiffness is actually less than that of the contact places limits on the accuracy with which specimen properties can be measured. Clearly, as the disparity between the stiffness of the instrument and the stiffness of the contact decreases, the more important it becomes to precisely know the stiffness of the instrument in order to accurately isolate the material's response. The same is also true for the damping of the contact in comparison with the damping of the instrument.

### 3.1. Instrument characterization

Regardless of the type of instrumentation, accurate and precise measurements of $E'$ and $E''$ are critically dependent on the ability to correctly measure and model the frequency response of the test equipment. While the characterization techniques discussed in this section are specific to the instrument used in this study the general concepts are applicable to all types of instrumentation, regardless of the manufacturer.

Figure 2(*a*) shows a schematic illustration of the head design of the instrument and the simple harmonic oscillator model used to predict its frequency response. For the purposes of this discussion, it is important to note the following features: the load is controlled by electromagnetic actuation, the displacement is measured using the parallel plate capacitive gauge, and the indenter column is supported by two leaf springs with a vertical stiffness of approximately 100 N m$^{-1}$ and a lateral stiffness of approximately 10 000 N m$^{-1}$. Among the most important aspects of the head design is that the lateral stiffness of the support springs effectively limits the system to only 1 degree of freedom, i.e. vertical motion. This physical limit is imperative in order for the oscillator model to be an accurate reflection of the physical motion of the indenter. However, because the remaining degrees of freedom each have their own frequency response, there will be a cutoff frequency above which cross-talk and/or phase rotations caused by other modes of vibration effectively prevent accurate instrument characterization. Thus, accurate measurements can only be made below the cutoff frequency. Also, of significant importance is knowledge that eddy currents in the voice coil as well as moving air through the 2 mm gap of the capacitance gauge generate sufficient damping such that the instrument is over critically damped. In addition to being dependent on frequency, the dynamic stiffness and damping of the instrument are also a function of the physical location of the centre plate relative to its full range of travel in the capacitance gauge. To simplify further discussion of this positional dependence, the centre plate's position in the gap is called the raw displacement and the centre of the gap is taken to be the zero datum (0 nm). Generally speaking, it is good experimental practice to mount the samples in the instrument such that the raw displacement at the surface of the sample is within $\pm$100 000 nm of 0 nm. This range in the capacitance gauge corresponds to nearly constant stiffness and damping at a given frequency. Complete dynamic characterization of the instrument consists of measuring the reference phase angle as a function of frequency, and measuring the stiffness and damping as a function of frequency and raw displacement.

*3.1.1. Determining the cutoff frequency.* Because other modes of vibration come into play at high frequencies, cross-talk and/or phase rotations can affect the frequency response of the instrument in a manner that is not described or accounted for in the simple one-dimensional oscillator model shown in figure 2(*a*). As a result, this additional motion makes it impossible to accurately determine the dynamic stiffness and damping of the instrument. Therefore, this cutoff frequency must be experimentally identified and not exceeded in any characterization work. One way to identify the cutoff is to measure the phase angle as a function of frequency with the indenter free hanging in space. Figure 3(*a*) shows the phase angle as a function of frequency for the indentation system used in this work. The smooth region of the curve, from 1 to 50 Hz, indicates frequencies consistent with the one-dimensional oscillator model. The discontinuity at 53 Hz indicates the cutoff frequency, beyond which cross-talk and/or phase rotations from other modes of vibration contribute to the measured response in a manner that is not modelled. Therefore, accurate characterization of the instrumentation, and hence the complex modulus of the sample, can be made only over the frequency range of approximately 1–50 Hz.

*3.1.2. Measuring the reference phase angle.* The dynamic measurements performed with the CSM technique are carried out using a frequency-specific phase-lock amplifier or PLA. As the command signal for the harmonic load travels through filters in the PLA, a phase shift that varies almost linearly as a function of frequency is introduced. During an experiment, accurate measurement of the phase angle between the applied harmonic load and the resulting harmonic displacement therefore depends on correcting the measured phase angle for the filter-induced phase shift.

Applying a large load (3 mN) oscillation to reduce the signal to noise ratio, the phase angle between the applied load

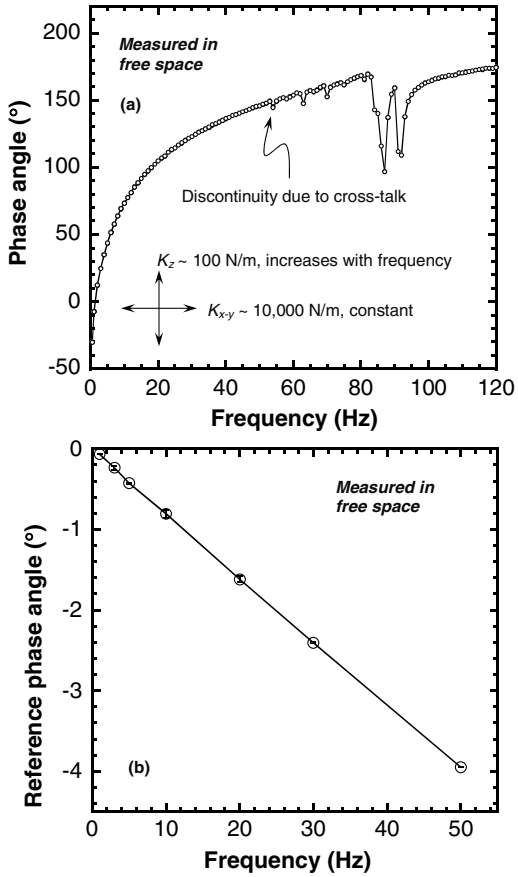


**Figure 3.** (*a*) The phase angle as a function of frequency, measured in increments of 1 Hz with the indenter column hanging in free space. The discontinuity at 53 Hz indicates the point at which the difference in stiffness between the $z$ and $x$–$y$ plane is no longer large enough to prevent (cross-talk cross-talk and/or phase rotation). (*b*) The reference phase angle as a function of frequency, measured with the indenter column hanging in free space and at the same frequencies to be used in characterizing the sample (filter induced phase shift).

and the load leaving the PLA is easily measured as a function of frequency. Figure 3(*b*) shows the average of 15 measurements of this reference phase angle over the range 1–50 Hz. The error bars span one standard deviation about the mean. The reference phase angle is used to correctly configure the PLA at each frequency during the experiment.

*3.1.3. Measuring the dynamic stiffness and damping of the testing system.* In order to maximize the accuracy of the measured $E'$ and $E''$, it is necessary that the instrument and sample characterization be performed at or near the same raw displacement, since the stiffness and damping of the instrument are a function of position, particularly towards the extreme ends of travel. Thus, in terms of the chronological flow of the experiment, the dynamic stiffness and damping can be measured only after determining the approximate raw displacement at which the sample characterization will subsequently take place. A number of factors affect the determination of the appropriate raw displacement to perform the sample characterization, as it depends on the choice of indenter geometry and ultimately, the necessity to generate a

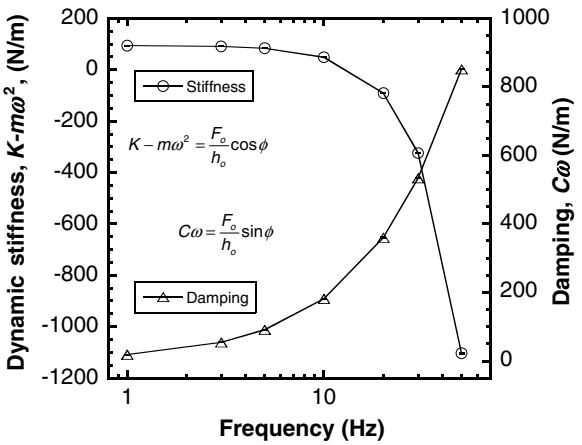


**Figure 4.** The dynamic stiffness and damping of the testing system as a function of frequency, measured with the indenter column hanging in free space and at the same frequencies to be used in characterizing the sample. The indenter is positioned at the raw displacement (position in the capacitance gauge) that corresponds to full contact (measured stiffness and damping in free space, raw disp. $= 18.8\,\mu$m).

contact representative of linear viscoelasticity. These factors will be discussed in detail in section 3.2.

With the indenter tip hanging in free space and positioned at the approximate raw displacement at which the sample characterization will take place, the stiffness and damping of the instrument are measured as a function of frequency using equations (12) and (13). Clearly, these measurements must be performed with the PLA correctly configured with the previously measured reference phase angles. Figure 4 shows the measured stiffness and damping of the testing system at each frequency that will be used to characterize the sample. These data represent the average of 15 measurements. The error bars span one standard deviation about the mean. Among the notable features in these data are the excellent reproducibility, and beyond resonance (14.3 Hz), the rapid increase in the magnitude of the dynamic stiffness. Consistent with the oscillator model and the phasor diagram in figure 1(*b*), the dynamic stiffness goes to zero and the phase angle goes to 90° at the resonant frequency. Beyond resonance, the dynamic stiffness is negative because the phase angle is in excess of 90°.

The data presented in figure 4 may also be used to experimentally confirm the validity of the assumed dynamic model of the instrument (figure 2(*a*)). Assuming the model is an accurate description of the physical motion of the system, then adding $m\omega^2$ to both sides of equation (12) and dividing both sides of equation (13) by $\omega$ will produce constant values as a function of frequency for both the support spring stiffness $K_s$ and the damping coefficient $C$. Using the data acquired at 1 and 50 Hz in conjunction with equation (12), the mass was found to be 12.14 g. For each of the seven frequencies, adding the $m\omega^2$ term back into the stiffness and dividing the damping by $\omega$ led to an average stiffness of 98 N m$^{-1}$ ± 4.9% and an average damping coefficient of 2.9 Ns m$^{-1}$ ± 2.5%. The fact that these values are relatively constant as a function of frequency clearly demonstrates that the simple harmonic oscillator accurately describes the physical motion of the system.

### *3.2. Measurement of the complex modulus by dynamic nanoindentation*

In order to accurately measure $E'$ and $E''$, the dynamic indentation experiment must achieve steady-state harmonic motion while the instrument and sample are coupled through a known contact geometry. In addition, the resulting stress and strain must be representative of linear viscoelasticity. Once the tip geometry has been chosen, these three criteria shape the design of the indentation experiment. As such, the purpose of this section is to develop an indentation test method that optimizes the accuracy and precision of the measured $E'$ and $E''$. The results presented in this section were calculated in accordance with the procedure outlined in section 2.3.

*3.2.1. Determining full contact with the flat punch.* Among the reasons for choosing the flat punch indenter geometry are (1) it effectively eliminates uncertainty in the contact area and (2) it avoids the problem of achieving steady-state harmonic motion in the presence of transient behaviour. However, the flat punch is not without its drawbacks, the most significant of which is that the punch cannot be mounted perfectly normal to the test surface. There is always a small angle between the face of the punch and the surface of the sample. As a result, the test method must have a robust means of identifying the point at which the face of the punch is brought in full contact with the surface of the sample. In addition, the punch geometry also creates a stress concentration along the circumference of the contact. It is assumed that the contribution of the stress concentration to the measured dynamic stiffness and damping is negligible. However, this has not been confirmed experimentally.

Figure 5 presents data from a single experiment and shows the harmonic displacement and phase angle as a function of raw displacement. For the sake of clarity, only 5% of the data are plotted. Both the harmonic displacement and phase angle can be used as a reliable indicator of the point of contact, since the drop in both signals occurs precisely when the punch makes contact with the surface of the sample. The criterion for full contact between the face of the punch and surface of the sample is thus based on the harmonic displacement and its establishment of a stable, constant value.

*3.2.2. Generating steady-state harmonic motion.* A fundamental assumption in modelling the combined dynamic response of the instrument and sample (figure 2(*b*)) is that of a steady-state harmonic response. In order for the model to be an accurate reflection of the physical experiment, transient behaviour must be given enough time to dissipate such that its effect on the dynamic response is negligible. For example, in a load-amplitude controlled experiment performed with a pointed indenter or sphere, creep behaviour will cause the contact area to increase with time, which in turn will cause the displacement amplitude to decrease until the creep transient dissipates. Only once the transient is removed is the model presented in figure 2(*b*) an accurate reflection of the experiment.

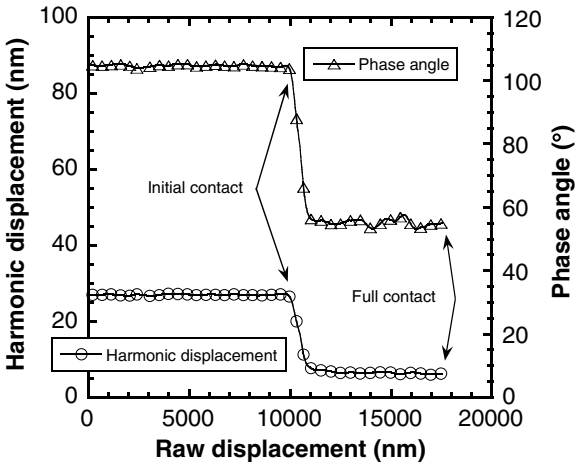


**Figure 5.** The harmonic displacement and phase angle as a function of raw displacement. These data are used to determine the raw displacement at both the point of initial contact and full contact between the face of the punch and the surface of the sample. The criterion for initial contact is a specified change in the phase angle. The criterion for full contact is a specified time rate of change in the harmonic displacement.

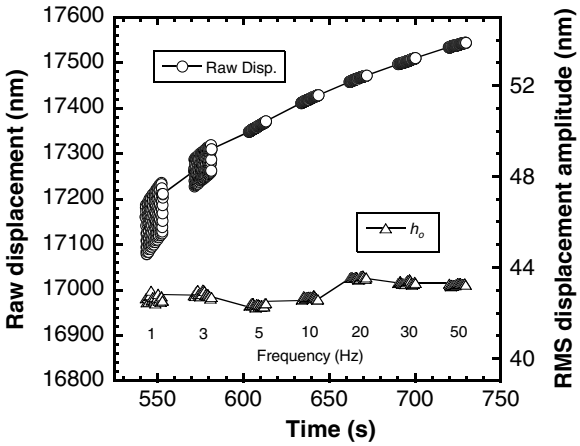


**Figure 6.** The raw displacement and oscillation amplitude as a function of time for a typical measurement performed on the sample. At each frequency, the harmonic load is different but fixed. The resulting oscillation amplitude is constant at each frequency only because the contact area does not change, despite the transient behaviour in the raw displacement (steady-state harmonic motion).

A distinct advantage of the flat punch geometry is that even in the presence of creep behaviour, the contact area cannot change, and hence, neither can the amplitude of the oscillation. However, if the creep rate is large enough, it is possible that the additional strain in the vicinity of the contact may be enough to violate the small strain assumption of linear viscoelasticity. This undesirable effect of creep may be easily avoided by monitoring the creep rate, while at the same time, periodically returning the indenter to the raw displacement corresponding to full contact. Until the measured creep rate falls below a specified level, the experiment continues to measure the creep rate and then return to the raw displacement at full contact. In this way, the raw displacement is maintained at the target position and the transient behaviour is given enough time to effectively dissipate.

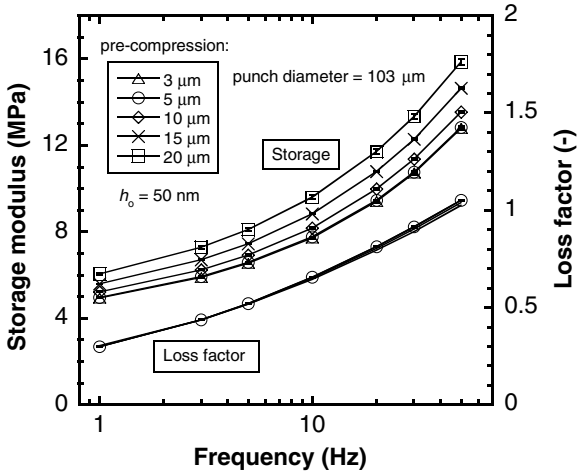


**Figure 7.** The storage modulus and loss factor as a function of frequency and static pre-compression distance. These data show that the static pre-compression distance must be less than 5 $\mu$m in order to generate data consistent with the assumptions of linear viscoelasticity (complex modulus as a function of static pre-compression).

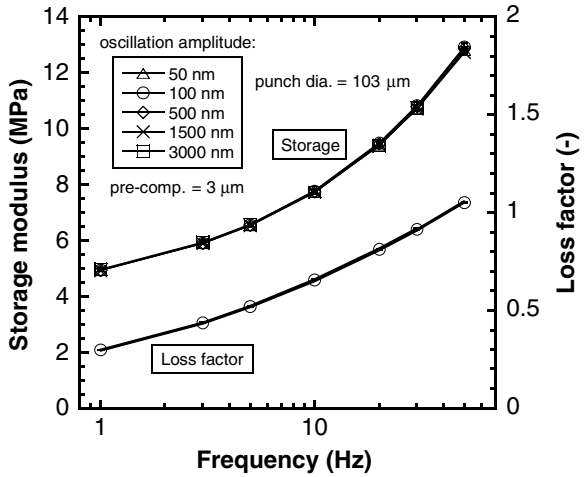


**Figure 8.** The storage modulus and loss factor as a function of frequency and oscillation amplitude. These data clearly show that oscillation amplitudes ranging from 50 to 3000 nm generate data consistent with the assumptions of linear viscoelasticity (complex modulus as a function of displacement oscillation amplitude).

Illustrating data from one experiment on the PVC, figure 6 shows the raw displacement and the RMS displacement amplitude as a function of time and frequency. The change in the raw displacement with time is due to creep. The increase in penetration depth over the duration of the experiment is approximately 490 nm. Despite this creep behaviour, the contact area is constant and hence the displacement amplitude is constant with time as well, as shown in the figure. It is important to note that the displacement oscillation is driven by a different, but constant force oscillation at each frequency. Because the force and displacement amplitude are both constant with time at each frequency, steady-state behaviour is achieved.

*3.2.3. Determining the linear viscoelastic regime.* In order to make a meaningful comparison between the DMA and nanoindentation test results, determination of $E'$ and $E''$ requires data representative of linear viscoelasticity. By definition, this means that an increase in the applied load or displacement amplitude has no effect on the measured $E'$ and $E''$. Therefore, only in the regime where the measured properties are constant as a function of static pre-compression (an increase in the applied load) and oscillation amplitude is the condition of linear viscoelasticity valid.

Figure 7 shows $E'$ and the loss factor as a function of frequency and static pre-compression. The oscillation amplitude was nominally 50 nm for all five compression distances. Because $\tan\phi$ is considered the fundamental measure of damping in a linear material, the remaining test results will be presented in terms of $E'$ and the loss factor. The data in figure 7 represent an average of 15 measurements, and the error bars span one standard deviation about the mean. For the sake of clarity, the loss factor is represented by the individual lines for each compression distance, but only one set of data markers are plotted. These results clearly show that compressing the sample up to an additional 5 $\mu$m beyond the point of full contact has no measurable effect on $E'$. However, between 5 and 10 $\mu$m of compression, the measured $E'$ begins to increase. Presumably, the increase is due to the additional static strain, thereby violating the small strain assumption of linear viscoelasticity. However, it is also possible that the surface of the sample has made partial contact with the sides of the punch. The fact that there is little to no measurable change in the loss factor indicates that $E''$ mirrors the change in $E'$. The picture that emerges is that additional static strain in the vicinity of the contact produces a proportional increase in the material's ability to store and dissipate energy such that there is no measurable change in the material's internal friction.

Figure 8 shows $E'$ and the loss factor as a function of frequency and oscillation amplitude. The compression distance is 3 $\mu$m beyond the point of full contact. The data represent an average of 15 measurements and the error bars span one standard deviation about the mean. These data clearly show that ranging the oscillation amplitude from 50 to 3000 nm has no measurable effect on the components of the complex modulus. Collectively, the experimental observations presented in figures 7 and 8 indicate that compressing the sample an additional 3 $\mu$m past the point of full contact and using a 50 nm oscillation amplitude results in data which are well within the limits of linear viscoelasticity.

*3.2.4. Comparing nanoindentation and DMA results.* Figure 9 presents a direct comparison of $E'$ and the loss factor of highly plasticized PVC (a bulk, high-damping thermoplastic) as determined by nanoindentation and DMA at 22 °C. Both the nanoindentation and DMA data represent the average of 15 measurements and the error bars span one standard deviation about the mean. Clearly, the two techniques produce similar results over the range 1–25 Hz. At 1 Hz, where the disparity in $E'$ is greatest, the difference between the two

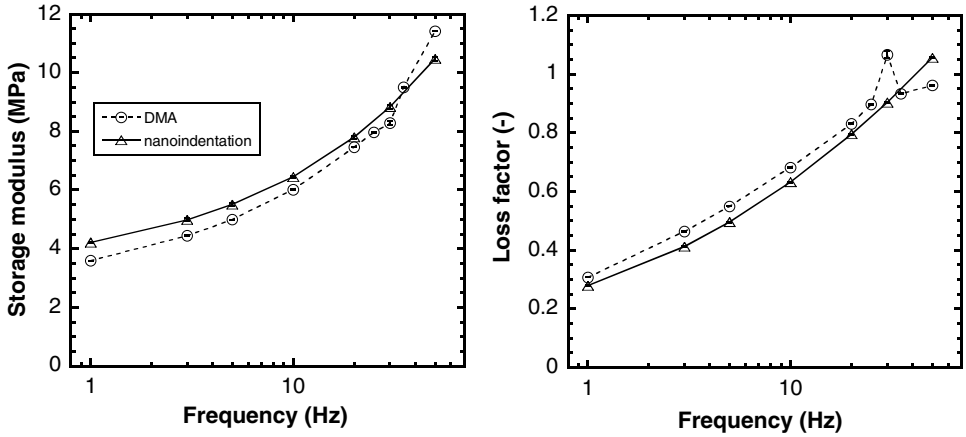


**Figure 9.** The complex modulus as a function of frequency as determined by dynamic nanoindentation and DMA (highly plasticized PVC at 22 °C).

techniques is still within 15%. Between 30 and 35 Hz, the DMA data unexpectedly break from the smooth curve for unknown reasons. Conversely, over the full frequency range 1–50 Hz, the nanoindentation data give a smooth curve that is consistent with expectations for the behaviour of a bulk, isotropic, homogeneous viscoelastic solid well above its glass transition temperature. While the nature of the discrepancy in the DMA data is unknown, it is important to recall that the instrument was completely calibrated in accordance with the procedure provided by TA Instruments. Nevertheless, in comparing the nanoindentation and DMA data, the clear message is the two characterization techniques produce very nearly the same results.

## 4. Summary and conclusions

The data presented in this work demonstrate the ability of nanoindentation to accurately and precisely measure the complex modulus of linear viscoelastic solids. Successful application of the technique requires rigorous characterization of the frequency response of the measurement system itself. For the measurement system used in this study, the crucial parameters are the reference phase angle of the phase-lock amplifier and the dynamic stiffness and damping of the instrument, both of which depend on the frequency of the measurement and the position of the centre plate in the capacitance gauge. Because of cross-talk and/or phase rotations, there is a cutoff frequency above which the instrument's frequency response cannot be accurately modelled. This cutoff frequency must be experimentally determined and not exceeded in any measurements. In order to confirm the accuracy of the nanoindentation test results, experimental verification should be provided to prove the data are representative of steady-state harmonic motion, a known contact geometry and linear viscoelasticity. Only under these conditions are the measured storage and loss modulus uniquely related to the transient functions from which they are derived, namely, creep and stress relaxation.

## Acknowledgments

The authors are particularly grateful for the input of Kermit Parks and Lee Spencer of the MTS Nano Instruments Innovation Center and Dr Mark Dadmun of the University of Tennessee. Tom Malmgren, also of UT, provided outstanding support in performing the DMA experiments.

## References

[1] Oliver W C and Pharr G M 2004 *J. Mater. Res.* **19** 3
[2] Hay J L and Pharr G M 2000 *ASM Handbook* **8** 232
[3] VanLandingham M R 2003 *J. Res. Natl Inst. Stand. Technol.* **108** 249
[4] Cheng L, Xia X, Yu W, Scriven L E and Gerberich W W 2001 *J. Polym. Sci. B: Polym. Phys.* **38** 10
[5] Larrson P-L and Carlsson S 1998 *Polym. Test.* **17** 49
[6] Shimizu S, Yanagimoto T and Sakai M 1999 *J. Mater. Res.* **14** 4075
[7] Sakai M 2002 *Phil. Mag.* A **82** 1841
[8] Oyen M L and Cook R F 2003 *J. Mater. Res.* **18** 139
[9] Bucaille J L, Felder E and Hochstetter G 2002 *J. Mater. Sci.* **37** 3999
[10] Ovaert T C, Kim B R and Wang J 2003 *Prog. Org. Coat.* **47** 312
[11] Huber N and Tyulyukovskiy E 2004 *J. Mater. Res.* **19** 101
[12] Cheng Y-T, Ni W and Cheng C-M 2005 *J. Mater. Res.* **20** 3061
[13] Loubet J-L, Lucas B N and Oliver W C 1995 *NIST Special Publication* **896** 31
[14] Lucas B N 1997 *PhD Dissertation* University of Tennessee, Knoxville
[15] Cheng Y-T, Ni W and Cheng C-M 2006 *Phys. Rev. Let.* **97** 075506
[16] Odegard G M, Gates T S and Herring H M 2005 *Exp. Mech.* **45** 130
[17] White C C, Drzal P L and VanLandingham M R 2005 *Mater. Res. Soc. Symp. Proc.* **841** R5.3
[18] Tweedie C A and Van Vliet K J 2006 *J. Mater. Res.* **21** 1576
[19] Lakes R S 1999 *Viscoelastic Solids* (Boca Raton, FL: CRC Press) p 63
[20] Sneddon I N 1965 *Int. J. Eng. Sci.* **3** 47
[21] King R B 1987 *Int. J. Solids Struct.* **23** 1657
[22] Wright W J, Maloney A R and Nix W D 2007 *Int. J. Surf. Sci. Eng.* **1** 274